



23 assessed its pathogenicity in hACE2 mice. We found that the GX\_P2V(short\_3UTR)  
24 clone can infect hACE2 mice, with high viral loads detected in both lung and brain  
25 tissues. This infection resulted in 100% mortality in the hACE2 mice. We surmise that  
26 the cause of death may be linked to the occurrence of late brain infection.

27 The GX\_P2V(short\_3UTR) mutant, initially isolated from the early passages of  
28 the GX\_P2V sample (6), and the GX\_P2V virus itself, have not been studied in terms  
29 of their adaptive mutations in cell cultures. To obtain a genetically homogenous clone  
30 for animal experiments, we cloned the passaged mutant through two successive plaque  
31 assays. Eight viral clones were chosen for next-generation sequencing (National  
32 Genomics Data Center of China, GSA: CRA014225). These clones, when compared  
33 with the genome of the original mutant (6), all shared four identical mutations:  
34 ORF1ab\_D6889G, S\_T730I, S\_K807N, and E\_A22D (Supporting Information, Table  
35 S1). Clone 7, named as GX\_P2V C7, was randomly selected for the evaluation of viral  
36 pathogenicity in hACE2 mice (Figure 1A). The hACE2 mouse model expressing  
37 human ACE2 under control of the CAG promoter was developed using random  
38 integration technology by Beijing SpePharm Biotechnology Company.

39 We initially assessed whether GX\_P2V C7 could cause disease in hACE2 mice by  
40 monitoring daily weight and clinical symptoms. A total of four 6 to 8-week-old hACE2  
41 mice were intranasally infected with a dosage of  $5 \times 10^5$  plaque-forming units (pfu) of  
42 the virus. Four mice inoculated with inactivated virus and four mock-infected mice  
43 were used as controls. Surprisingly, all the mice that were infected with the live virus  
44 succumbed to the infection within 7-8 days post-inoculation, rendering a mortality rate

45 of 100% (Figure 1B). The mice began to exhibit a decrease in body weight starting from  
46 day 5 post-infection, reaching a 10% decrease from the initial weight by day 6 (Figure  
47 1C). By the seventh day following infection, the mice displayed symptoms such as  
48 piloerection, hunched posture, and sluggish movements, and their eyes turned white.  
49 The criteria for clinical scoring of the mice and the daily clinical scores post-infection  
50 with GX\_P2V C7 are provided in the Supporting Information, Figure S1.

51 We then evaluated the tissue tropism of GX\_P2V C7 in hACE2 mice. Using the  
52 infection method described above, eight hACE2 mice were infected, eight mice were  
53 inoculated with inactivated virus, and another eight mock-infected mice were used as  
54 controls. The organs of four randomly selected mice in each group were dissected on  
55 days 3 and 6 post-infection for quantitative analysis of viral RNA and titer. We detected  
56 significant amounts of viral RNA in the brain, lung, turbinate, eye, and trachea of the  
57 GX\_P2V C7 infected mice (Figure 1D), whereas no or a low amount of viral RNA was  
58 detected in other organs such as the heart, liver, spleen, kidneys, tongue, stomach, and  
59 intestines. Specifically, in lung samples, we detected high viral RNA loads on days 3  
60 and 6 post-infection, with no significant difference between these two time points (~  
61 6.3 versus ~ 5.8 Log<sub>10</sub>[copies/mg]). In brain samples, on day 3 post-infection, viral  
62 RNA was detected in all four infected mice, with an average value of 5.4  
63 Log<sub>10</sub>[copies/mg]. Notably, by day 6 post-infection, we detected exceptionally high  
64 viral RNA loads (~ 8.5 Log<sub>10</sub>[copies/mg]) in the brain samples from all four infected  
65 mice (Figure 1D). On days 3 and 6 post-infection, the viral RNA loads in the turbinate  
66 were similar, approximately 4.1 and 3.9 Log<sub>10</sub>[copies/mg], respectively. The viral RNA

67 loads in the trachea and eyes of the mice surpassed the limit of detection only on day 6  
68 post-infection, with values of 2.6 and 3.8  $\text{Log}_{10}[\text{copies}/\text{mg}]$ , respectively. Regarding the  
69 infectious viral titers, lung tissues at day 3 post-infection had a value of  $\sim 1.8$   
70  $\text{Log}_{10}[\text{pfu}/\text{mg}]$ , which decreased to  $\sim 0.5 \text{Log}_{10}[\text{pfu}/\text{mg}]$  by day 6. Importantly, the  
71 highest infectious titers were detected in the brain on day 6, which was significantly  
72 greater than that on day 3 ( $\sim 0.9$  vs  $\sim 4.8 \text{Log}_{10}[\text{pfu}/\text{mg}]$ ) (Figure 1E). Additionally,  
73 there were no significant differences in the infectious titers in the turbinate between day  
74 3 ( $\sim 0.9 \text{Log}_{10}[\text{pfu}/\text{mg}]$ ) and day 6 ( $\sim 1.2 \text{Log}_{10}[\text{pfu}/\text{mg}]$ ) (Figure 1E). By day 6,  
75 approximately  $2.0 \text{Log}_{10}[\text{pfu}/\text{mg}]$  was detected in the eyes of two mice. Neither  
76 inactivated GX\_P2V C7 nor mock infection caused death or any clinical symptoms in  
77 the mice (Figure 1B-C and Supporting Information, Figure S2). In summary, in the mice  
78 infected with live virus, the viral load in the lungs significantly decreased by day 6;  
79 both the viral RNA loads and viral titers in the brain samples were relatively low on  
80 day 3, but substantially increased by day 6. This finding suggested that severe brain  
81 infection during the later stages of infection may be the key cause of death in these mice.

82 To determine the mechanisms underlying GX\_P2V C7-induced death in hACE2  
83 mice, we examined the pathological changes, presence of viral antigens, and cytokine  
84 profiles in the lung and brain tissues of the mice on days 3 and 6 post-infection (Figure  
85 1F-G, and Supporting Information, Figure S3 and S4). On both days, compared to those  
86 of control mice, the lungs of infected mice showed no significant pathological  
87 alterations, with only minor inflammatory responses due to slight granulocyte  
88 infiltration (Figure 1F). On day 3 post-infection, shrunken neurons were visible in the

89 cerebral cortex of the mice. By day 6, in addition to the shrunken neurons, there was  
90 focal lymphocytic infiltration around the blood vessels, although no conspicuous  
91 inflammatory reaction was observed (Figure 1G). Upon staining for viral nucleocapsid  
92 protein via immunohistochemistry, viral antigens were detected in both the lungs and  
93 brains on days 3 and 6 post-infection, with extensive viral antigens notably present in  
94 the brain on day 6 (Figure 1F-G). These findings align with the viral RNA load  
95 assessments in the lung and brain tissues (Figure 1D). We also performed a Luminex  
96 cytokine assay to detect 31 cytokines/chemokines in the lung and brain tissues of the  
97 mice (Supporting Information, Figure S3 and S4). Consistent with the pathological  
98 findings, there were slight increases or decreases in the levels of many  
99 cytokines/chemokines in lung and brain tissues compared to those in control tissues,  
100 but the levels of key inflammatory factors, such as IFN- $\gamma$ , IL-6, IL-1 $\beta$ , and TNF- $\alpha$ , did  
101 not significantly change. In brief, these analyses revealed that GX\_P2V C7 infection in  
102 hACE2 mice did not lead to severe inflammatory reactions, a finding that aligns with  
103 previous reports by Zhengli Shi's group using GX\_P2V infection in two different  
104 hACE2 mouse models (5), as well as our own findings in the golden hamster model (6).

105 To the best of our knowledge, this is the first report showing that a SARS-CoV-2-  
106 related pangolin coronavirus can cause 100% mortality in hACE2 mice, suggesting a  
107 risk for GX\_P2V to spill over into humans. Our findings are evidently inconsistent with  
108 those of Zhengli Shi *et al.* (5), who tested the virulence of GX\_P2V in two different  
109 hACE2 mouse models. It is important to note that we did not isolate the wild-type  
110 GX\_P2V strain. The study by Zhengli Shi *et al* tested the GX\_P2V(short\_3UTR)

111 variant that we reported. However, the adaptative evolutionary changes of this variant  
112 during their laboratory culture remain understudied. In fact, according to additional  
113 infection experiments, the uncloned GX\_P2V(short\_3UTR) also resulted in 100%  
114 mortality in hACE2 mice. Due to the propensity of coronaviruses to undergo adaptive  
115 mutation during passage culture, we cloned and analyzed mutations in  
116 GX\_P2V(short\_3UTR), focusing specifically on the pathogenicity of the cloned strains.  
117 The high pathogenicity mechanism of GX\_P2V C7 in hACE2 mice, in the absence of  
118 the wild-type GX\_P2V control, requires further investigation. Compared to the original  
119 sequence of GX\_P2V(short\_3UTR), GX\_P2V C7 has two amino acid mutations in the  
120 spike protein. Given the close relationship between coronavirus virulence and spike  
121 protein mutations (7), it is possible that GX\_P2V C7 has undergone a virulence-  
122 enhancing mutation. However, it is important to note that our hACE2 mouse model  
123 may be relatively unique. The company has not yet published a paper on this hACE2  
124 mouse model, but our results suggest that hACE2 may be highly expressed in the mouse  
125 brain. Additionally, according to the data provided by the company, these hACE2 mice  
126 have abnormal physiology, as indicated by relatively reduced serum triglyceride,  
127 cholesterol, and lipase levels, compared to those of wild-type C57BL/6J mice. In  
128 summary, our study provides a unique perspective on the pathogenicity of GX\_P2V  
129 and offers a distinct alternative model for understanding the pathogenic mechanisms of  
130 SARS-CoV-2-related coronaviruses.

131

132 Lai Wei<sup>1,#</sup>, Shuiqing Liu<sup>1,#</sup>, Shanshan Lu<sup>1,#</sup>, Shengdong Luo<sup>2</sup>, Xiaoping An<sup>1</sup>, Huahao

133 Fan<sup>1</sup>, Weiwei Chen<sup>2</sup>, Erguang Li<sup>3,\*</sup>, Yigang Tong<sup>1,\*</sup>, Lihua Song<sup>1,\*</sup>

134 <sup>1</sup> Beijing Advanced Innovation Center for Soft Matter Science and Engineering,

135 College of Life Science and Technology, Beijing University of Chemical Technology,

136 Beijing, China. <sup>2</sup>Research Center for Clinical Medicine, The Fifth Medical Center of

137 PLA General Hospital, Beijing, China. <sup>3</sup>State Key Laboratory of Pharmaceutical

138 Biotechnology, Medical School, Nanjing University, China

139 #Contributed equally.

140 \*email: [erguang@nju.edu.cn](mailto:erguang@nju.edu.cn); [tong.yigang@gmail.com](mailto:tong.yigang@gmail.com); [songlihua@gmail.com](mailto:songlihua@gmail.com)

141

## 142 REFERENCES

143 1. Liu P, Chen W, Chen JP. Viral Metagenomics Revealed Sendai Virus and

144 Coronavirus Infection of Malayan Pangolins (*Manis javanica*). *Viruses*. 2019 Oct

145 24;11(11).

146 2. Lam TT, Jia N, Zhang YW, Shum MH, Jiang JF, Zhu HC, et al. Identifying SARS-

147 CoV-2-related coronaviruses in Malayan pangolins. *Nature*. 2020 Jul;583(7815):282-5.

148 3. Xiao K, Zhai J, Feng Y, Zhou N, Zhang X, Zou JJ, et al. Isolation of SARS-CoV-

149 2-related coronavirus from Malayan pangolins. *Nature*. 2020 Jul;583(7815):286-9.

150 4. Huang XY, Chen Q, Sun MX, Zhou HY, Ye Q, Chen W, et al. A pangolin-origin

151 SARS-CoV-2-related coronavirus: infectivity, pathogenicity, and cross-protection by

152 preexisting immunity. *Cell Discov*. 2023 Jun 17;9(1):59.

153 5. Liu MQ, Lin HF, Li J, Chen Y, Luo Y, Zhang W, et al. A SARS-CoV-2-Related

154 Virus from Malayan Pangolin Causes Lung Infection without Severe Disease in Human

155 ACE2-Transgenic Mice. *J Virol*. 2023 Feb 28;97(2):e0171922.

156 6. Lu S, Luo S, Liu C, Li M, An X, Li M, et al. Induction of significant neutralizing  
157 antibodies against SARS-CoV-2 by a highly attenuated pangolin coronavirus variant  
158 with a 104nt deletion at the 3'-UTR. *Emerg Microbes Infect.* 2023 Dec;12(1):2151383.

159 7. Roberts A, Lamirande EW, Vogel L, Jackson JP, Paddock CD, Guarner J, et al.  
160 Animal models and vaccines for SARS-CoV infection. *Virus Res.* 2008 Apr;133(1):20-  
161 32.

162

### 163 **ACKNOWLEDGEMENTS**

164 This work was supported by NSFC-MFST project (China–Mongolia) (grant number  
165 32161143027), National Key R&D Program of China (2021YFC2301804) and  
166 Biosafety Special Program (No. 19SWAQ 13).

### 167 **ETHICS STATEMENT**

168 All animals involved in this study were housed and cared for in an AAALAC  
169 (Association for Assessment and Accreditation of Laboratory Animal Care) accredited  
170 facilities. The procedure for animal experiments (IACUC-2019-0027) was approved by  
171 the Institutional Animal Care and Use Committee of the Fifth Medical Center, General  
172 Hospital of the Chinese People's Liberation Army, and complied with IACUC standards.

### 173 **AUTHOR CONTRIBUTIONS**

174 L.Song conceived and designed the study and wrote the manuscript. L.W., S.Liu, S.Lu.,  
175 and S.Luo. performed the experiments and analyzed the data. X.A., H.F., W.C., E.L.  
176 and Y.T. analyzed the data and edited the manuscript. L.W. and L.Song wrote the  
177 manuscript and all the authors approved the manuscript.



178 **CONFLICT OF INTERESTS**

179 The authors declare no competing interests.

180 **SUPPORTING INFORMATION**

181 Additional Supporting Information for this article can be found online at

182 **DATA AVAILABILITY**

183 All the data supporting the findings of this study are available within the article and  
184 the Supporting Information, or from the corresponding author upon reasonable  
185 request.

186 **ORCID**

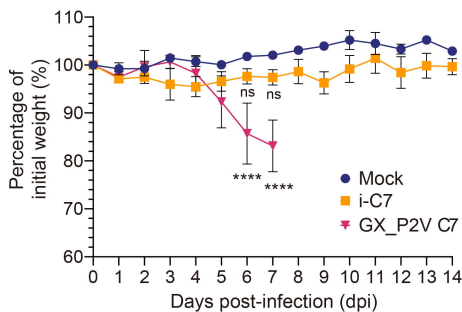
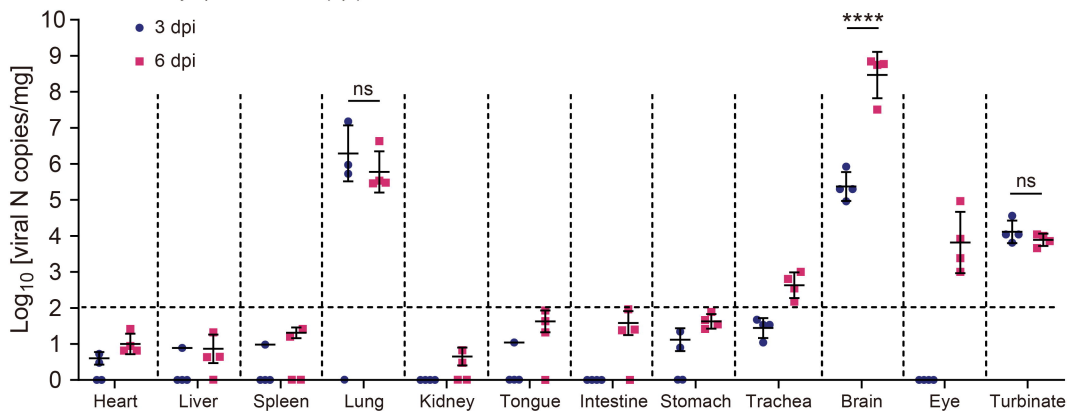
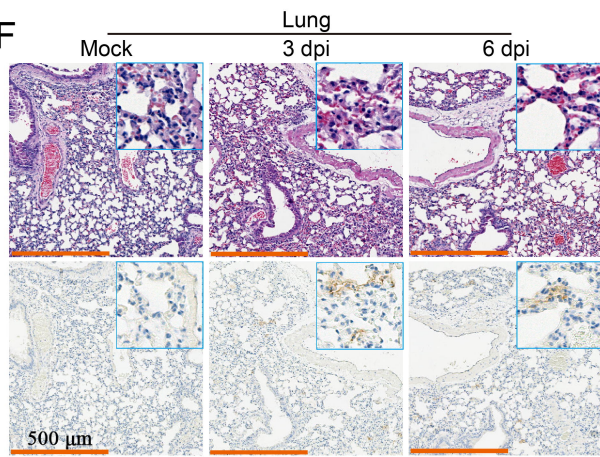
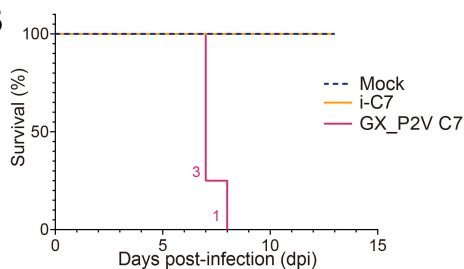
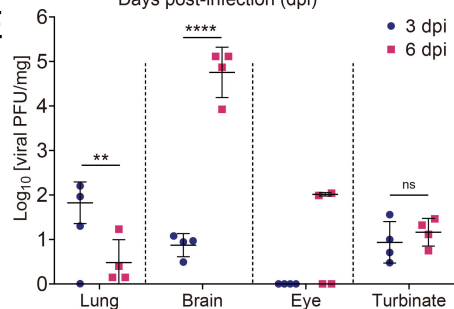
187 Lihua Song, <https://orcid.org/0000-0002-7299-5719>

188 **Figure 1: Characterization of a lethal infection model in human ACE2-transgenic**  
189 **mice caused by the attenuated SARS-CoV-2-related pangolin coronavirus**  
190 **GX\_P2V C7. A** Mutations in GX\_P2V C7 compared to the GX\_P2V(short\_3UTR)  
191 isolate (NCBI accession number: MW532698). The four identical mutations are shown  
192 in bold. **B** Survival of hACE2 transgenic mice following intranasal infection with  
193 GX\_P2V C7 ( $n = 4$ ), inactivated GX\_P2V C7 (i-C7,  $n = 4$ ), and mock infection ( $n = 4$ ).  
194 The number of deceased mice on each specific day is annotated on the left of the  
195 survival curve. **C** Percentage of initial weight of hACE2 transgenic mice after intranasal  
196 infection with GX\_P2V C7 ( $n = 4$ ), i-C7 ( $n = 4$ ), and mock infection ( $n = 4$ ). The  
197 statistical significance of the differences between mock-infected ( $n = 4$ , blue dots) and  
198 GX\_P2V C7-infected ( $n = 4$ , red dots) or i-C7-infected mice ( $n = 4$ , orange dots) at 6  
199 or 7 dpi are shown. The error bars represent the means  $\pm$  SDs. **D** Quantification of  
200 GX\_P2V N gene copies in heart, liver, spleen, lung, kidney, tongue, intestine, stomach,  
201 trachea, brain, eye, and turbinate homogenates at 3- and 6-day post-infection (dpi) ( $n =$   
202 4 per group). The limit of detection (LOD) for viral RNA loads in the original samples  
203 was  $\text{Log}_{10}[10^2 \text{ copies/mg}]$ . The error bars represent the means of  $\text{Log}_{10}[\text{copies/mg}] \pm$   
204 SDs. The significances of the comparisons in the lung, brain, and turbinate are shown.  
205 **E** Infectious viral titers in lung, brain, eye, and turbinate homogenates were measured  
206 by plaque forming assay at 3 and 6 dpi ( $n = 4$  per group). The statistical significance of  
207 the differences in the lung, brain, and turbinate are shown. The error bars represent  
208 means of  $\text{Log}_{10}[\text{pfu/mL}] \pm$  SDs. **F, G** Hematoxylin and eosin (H&E) staining and  
209 immunohistochemical (IHC) staining with an anti-SARS-CoV-2 N-specific antibody

210 (SARS-CoV-2) revealed viral antigen–positive cells (brown) in the lung (**F**) and brain  
211 (**G**), as shown at high magnification in the inset. Scale bars, 500  $\mu\text{m}$  (**F**) and 1 mm (**G**),  
212 respectively. \* $P < 0.05$ , \*\* $P < 0.01$ , \*\*\* $P < 0.001$ , \*\*\*\* $P < 0.0001$ ,  $P > 0.05$ , not  
213 significant (ns); two-way ANOVA followed by Sidak’s multiple comparison test.

**A**

Mutation	Codon change	Substitution	CDS Location
1807 A to G	GGA to GGG		ORF1ab
6501 C to U	ACA to AUA	T to I	ORF1ab
19694 C to U	ACA to AUA	T to I	ORF1ab
20930 A to G	GAU to GGU	D to G	ORF1ab
23727 C to U	ACU to AUU	T to I	S
23959 A to C	AAA to AAC	K to N	S
26274 C to A	GCU to GAU	A to D	E
29227 C to U	UAC to UAU		N

**C****D****F****B****E****G**